ACS chemical biology

Articles

Cite This: ACS Chem. Biol. 2018, 13, 2728−2738

pubs.acs.org/acschemicalbiology

Biochemical and Structural Characterization of TtnD, a Prenylated FMN-Dependent Decarboxylase from the Tautomycetin Biosynthetic Pathway

Thibault Annaval,[†] Lu Han,[‡] Jeffrey D. Rudolf,[†] Guangbo Xie,[†,#] Dong Yang,[†] Chin-Yuan Chang,[†] Ming Ma,[†,@] Ivana Crnovcic,[†] Mitchell D. Miller,[‡] Jayashree Soman,[‡] Weijun Xu,[‡] George N. Phillips, Jr.,[‡,§] and Ben Shen*[,†,∥,⊥]

[†]Department of Chemistry, The Scripps Research Institute, 130 Scripps Way, Jupiter, Florida 33458, United States

[‡]Department of BioSciences and [§]Department of Chemistry, Rice University, 6100 Main Street, Houston, Texas 77251, United States

[∥]Department of Molecular Medicine and [⊥]Natural Products Library Initiative at The Scripps Research Institute, The Scripps Research Institute, 130 Scripps Way, Jupiter, Florida 33458, United States

Supporting Information

ABSTRACT: Tautomycetin (TTN) is a polyketide natural product featuring a terminal alkene. Functional characterization of the genes within the *ttn* gene cluster from *Streptomyces griseochromogenes* established the biosynthesis of the TTN polyketide backbone, its dialkylmaleic anhydride moiety, the coupling of the two moieties to form the nascent intermediate TTN F-1, and the tailoring steps converting TTN F-1 to TTN. Here, we report biochemical and structural characterization of TtnD, a prenylated FMN (prFMN)-dependent decarboxylase belonging to the UbiD family that catalyzes the penultimate step of TTN biosynthesis. TtnD catalyzes decarboxylation of TTN D-1 to TTN I-1, utilizing prFMN as a cofactor generated by the TtnC flavin prenyltransferase; both TtnD and TtnC are encoded within the *ttn* biosynthetic gene cluster. TtnD exhibits substrate promiscuity but accepts only TTN D-1 congeners that feature an α,β-unsaturated acid, supporting the [3+2] cycloaddition mechanism during catalysis that requires the double bond of an α,β-unsaturated acid substrate. TtnD shares a similar overall structure with other members of the UbiD family but forms a homotetramer in solution. Each protomer is composed of three domains with the active site located between the middle and C-terminal domains; R169-E272-E277, constituting the catalytic triad, and E228, involved in Mn(II)-mediated binding of prFMN, were confirmed by site-directed mutagenesis. TtnD represents the first example of a prFMN-dependent decarboxylase involved in polyketide biosynthesis, expanding the substrate scope of the UbiD family of decarboxylases beyond simple aromatic and cinnamic acids. TtnD and its homologues are widespread in nature and could be exploited as biocatalysts for organic synthesis.

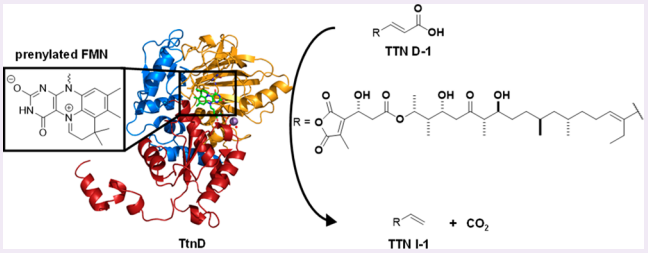

Tautomycetin (TTN) is a polyketide natural product featuring a terminal alkene (Figure 1). First isolated from *Streptomyces griseochromogenes* because of its antifungal activity,[1,2] TTN is a noteworthy serine/threonine protein phosphatase (PP) inhibitor and a potent immunosuppressant.[3−6] With a strong preference for PP-1 over PP-2A, TTN is the most selective PP-1 inhibitor known to date.[7] TTN is also a potent inhibitor of the Src homology-2 domain-containing protein tyrosine phosphatase-2 (SHP2).[8] The *ttn* biosynthetic gene cluster has been cloned and sequenced from *S. griseochromogenes*[9] and *Streptomyces* sp. CK4412.[10] Functional characterization of the TTN biosynthetic machinery has led to a proposal including (i) biosynthesis of the nascent polyketide backbone from five molecules of malonyl-CoA, four molecules of methylmalonyl-CoA, and one molecule of ethylmalonyl-CoA by TtnAB, (ii) formation of the dialkylmaleic anhydride moiety from α-ketoglutarate and propionate by TtnMOPR, (iii) coupling between the polyketide and dialkylmaleic anhydride moieties to afford the first characterized biosynthetic intermediate TTN F-1 by TtnK, and (iv) conversion of TTN F-1 to TTN via successive dehydration, decarboxylation, and oxidation of TTN F-1 by TtnF, TtnD, and TtnI, respectively (Figure 1).[9,11,12] Inactivation of *ttnD* in *S. griseochromogenes* afforded the Δ*ttnD* mutant SB13013 in which our metabolites accumulated, TTN D-1, TTN D-2, TTN D-3, and TTN D-4, all of which retained the terminal carboxylic acid. TtnD was therefore proposed to be a decarboxylase responsible for the installation of the terminal alkene of TTN by decarboxylating an α,β-unsaturated acid (Figure 1).[11,12]

Received: July 18, 2018
Accepted: August 28, 2018
Published: August 28, 2018

DOI: 10.1021/acschembio.8b00673
ACS Chem. Biol. 2018, 13, 2728−2738

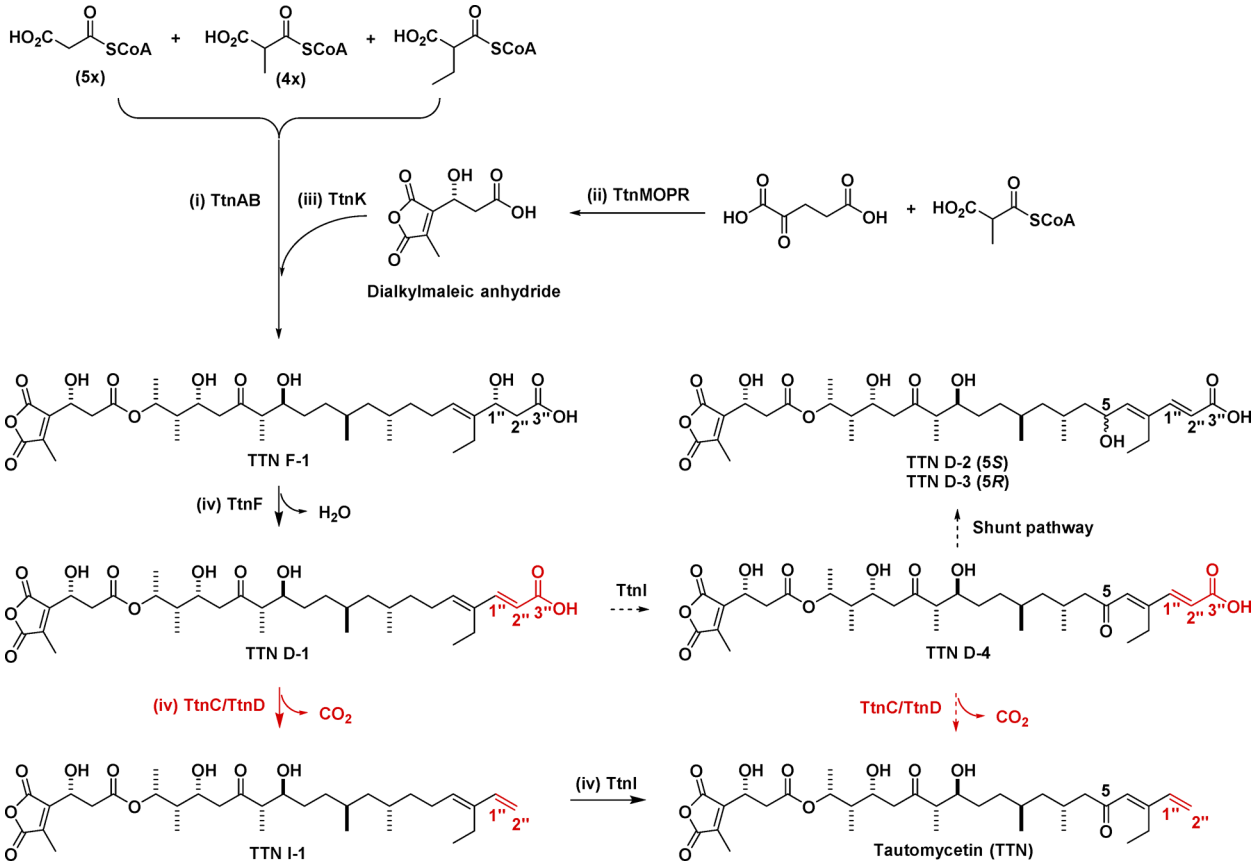

Figure 1. Proposed biosynthetic pathway for TTN in *S. griseochromogenes*.[9,11,12] (i) TtnAB catalyze the assembly of the TTN polyketide backbone. (ii) TtnMOPR catalyze the biosynthesis of the dialkylmaleic anhydride moiety. (iii) TtnK catalyzes the coupling between the polyketide and dialkylmaleic anhydride moieties to afford nascent intermediate TTN F-1. (iv) TtnF, TtnD, and TtnI successively catalyze dehydration, decarboxylation, and oxidation of TTN F-1 to complete TTN biosynthesis. Solid and dashed arrows represent the major and minor pathways, respectively. TTN D-2 and TTN D-3, which result from the reduction of TTN D-4, are adventitious metabolites isolated from the fermentation of Δ*ttnD* mutant SB13013. TtnD, which catalyzes the decarboxylation of *α,β*-unsaturated acids and requires the prFMN cofactor provided by TtnC, is colored red (see Figure 2).

Decarboxylation is one of the most common and fundamental reactions in nature.[13] Because of the high-energy barrier of the carbanion intermediate, many decarboxylases require cofactors such as flavins, pyridoxal phosphate, thiamine pyrophosphate, or divalent metal ions; only a few have been shown to catalyze decarboxylation without a cofactor.[13−16] UbiD is a well-known decarboxylase from *Escherichia coli* involved in ubiquinone biosynthesis, which catalyzes the decarboxylation of an aromatic acid, i.e., transforming 3-polyprenyl-4-hydroxybenzoic acid into 2-polyprenylphenol (Figure 2a).[17] Related by sequence is the ferulic acid decarboxylase (Fdc1), a homologue of UbiD from *Aspergillus niger*, which catalyzes the decarboxylation of several *α,β*-unsaturated acids, specifically substituted cinnamic acids, to afford the corresponding substituted styrenes (Figure 2a).[18] Very recently, it has been discovered that both UbiD and Fdc1 require a prenylated FMN (prFMN) for their decarboxylase activity, and the novel prFMN cofactor is biosynthesized from $FMNH_2$ and dimethylallyl monophosphate (DMAP) by the flavin prenyltransferase UbiX or Pad1 from the ubiquinone or ferulic acid biosynthetic pathway, respectively (Figure 2b).[19−22] Subsequent mechanistic and structural characterizations of UbiD and Fdc1 have culminated in a mechanism involving an unprecedented biological [3+2] cycloaddition between $prFMN^{iminium}$, the oxidized form of prFMN, and the double bond of the *α,β*-unsaturated acid substrate to account for the reversible decarboxylation catalyzed by these enzymes (Figure 2c).[19−28] Characterization of prFMN-containing decarboxylases acting on substrates other than benzoic acids, as exemplified by UbiD, or cinnamic acids, as exemplified by Fdc1, would further substantiate this unprecedented mechanism, expanding the catalytic landscape of this emerging family of novel enzymes (Figure 2).[14−16]

Here, we report biochemical and structural characterizations of the TtnD decarboxylase from the TTN biosynthetic machinery in *S. griseochromogenes*.[9,11,12] We revealed that (i) TtnD catalyzes decarboxylation of aliphatic *α,β*-unsaturated acids, utilizing prFMN as a cofactor generated by the TtnC flavin prenyltransferase, and both TtnC and TtnD are encoded within the *ttn* gene cluster, (ii) TtnD exhibits substrate promiscuity, accepting TTN D-1, the biosynthetic intermediate for TTN, as well as TTN D-2, TTN D-3, and TTN D-4, minor metabolites isolated from Δ*ttnD* mutant SB13013, (iii) TtnD does not decarboxylate TTN F-1, supporting the [3+2] cycloaddition mechanism during catalysis that requires the double bond of an *α,β*-unsaturated acid substrate, and (iv) R169, E272, and E277 constitute the catalytic triad of TtnD, which is consistent with the crystal structure of TtnD and supported by site-directed mutagenesis. TtnD represents the first example of a prFMN-dependent decarboxylase involved in

DOI: 10.1021/acschembio.8b00673
ACS Chem. Biol. 2018, 13, 2728−2738

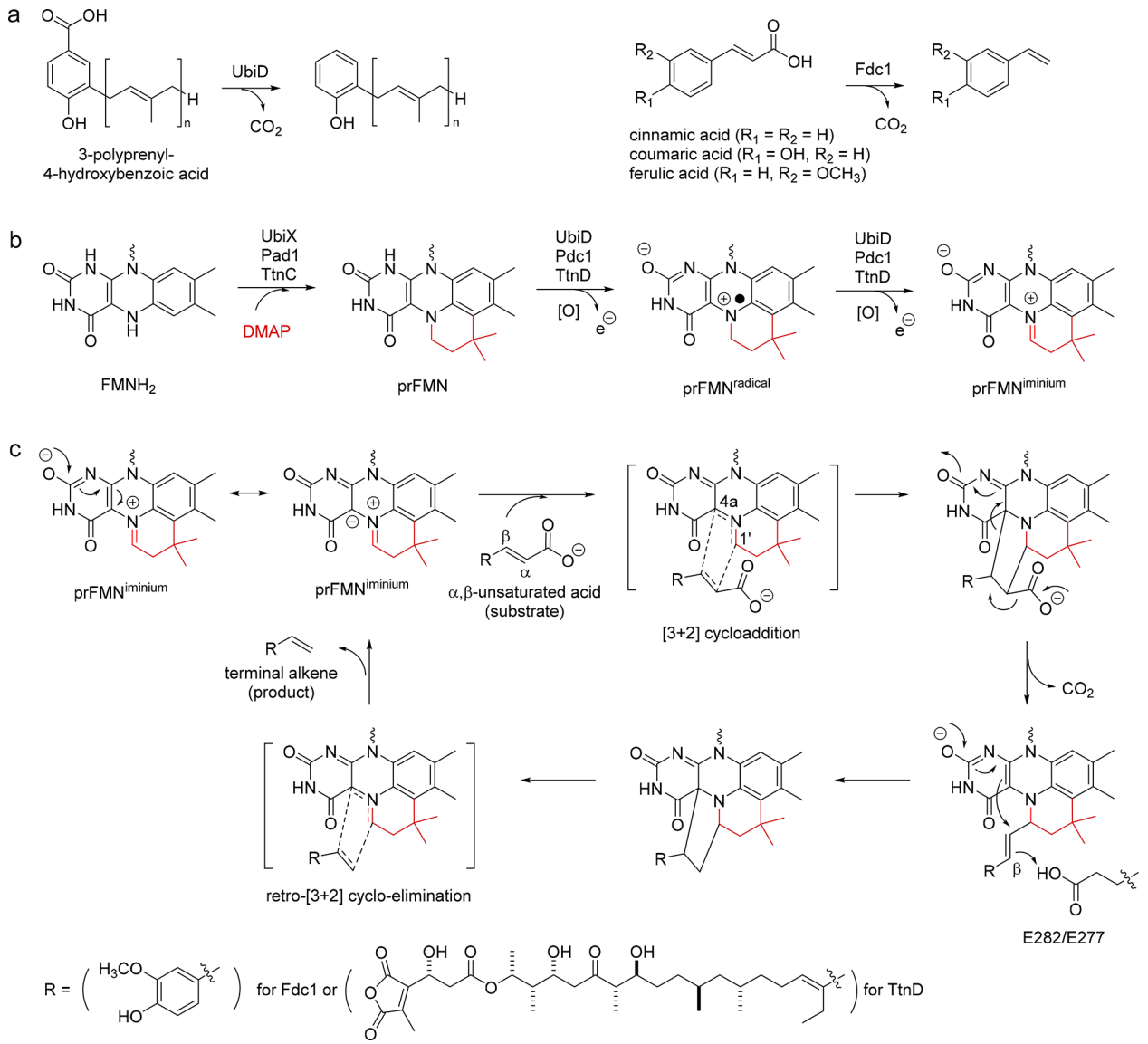

Figure 2. Decarboxylases characterized to date requiring a prenylated FMN as a cofactor.[15,16] (a) Decarboxylation of aromatic acids, as exemplified by UbiD, and of cinnamic acids, as exemplified by Fdc1,[19−28] in comparison with TtnD, which catalyzes the decarboxylation of aliphatic *α,β*-unsaturated acid TTN F-1. (b) Biosynthesis of prFMN from $FMNH_2$ and DMAP by flavin prenyltransferase UbiX or Pad1 and oxidation of prFMN into its active form, $prFMN^{iminium}$, in the presence of O_2 and UbiD or Fdc1,[20−22] in comparison with TtnC and TtnD. The $prFMN^{radical}$ form has been detected spectroscopically but is catalytically incompetent. (c) Proposed mechanism for prFMN-containing decarboxylase-catalyzed decarboxylation that involves an unprecedented biological [3+2] cycloaddition between $prFMN^{iminium}$ and the double bond of the *α,β*-unsaturated acid substrate.[19,23−28] After the [3+2] cycloaddition and subsequent decarboxylation, E282 and E277 from Fdc1 and TtnD, respectively, protonate the C*β* atom of the acyclic intermediate to form the second cyclic intermediate, setting the stage for the retro-[3+2] cyclo-elimination to release the alkene product and regenerate the $prFMN^{iminium}$ species. See Figure S1 for a comparison of the sequences of UbiD/Fdc1 and the TtnD decarboxylases.

polyketide biosynthesis, further expanding the catalytic repertoire of this emerging family of novel decarboxylases. TtnD and its homologues are widespread in nature and could be exploited as biocatalysts for organic synthesis.

RESULTS AND DISCUSSION

TtnC Flavin Prenyltransferase and Holo-TtnD. We previously mapped the timing of the tailoring steps for TTN biosynthesis by inactivating the *ttnF*, *ttnC*, *ttnD*, or *ttnI* genes in *S. griseochromogenes*, followed by isolation and structural characterization of the metabolites that accumulated in the corresponding mutant strain SB13014 (i.e., Δ*ttnF*),[11] SB13012 (i.e., Δ*ttnC*),[12] SB13013 (i.e., Δ*ttnD*),[11] or SB13017 (i.e., Δ*ttnI*),[12] respectively. Thus, while four metabolites, TTN D-1, TTN D-2, TTN D-3, and TTN D-4, accumulated in Δ*ttnD* mutant SB13013,[12] only TTN I-1 accumulated in Δ*ttnI* mutant SB13017, unambiguously establishing TtnD as a decarboxylase that catalyzed C-3″ decarboxylation of TTN D-1 to afford TTN I-1 as the penultimate step in TTN biosynthesis (Figure 1).[11,12] In contrast, Δ*ttnC* mutant SB13012 still produced TTN, with a titer comparable to that of the *S. griseochromogenes* wild type.[12] This was unexpected because TtnC was annotated at the time as a putative flavoprotein decarboxylase.[9,10] In the absence of any other experimental evidence, it was proposed then that TtnC played no essential role in TTN biosynthesis or its function could be

DOI: 10.1021/acschembio.8b00673
ACS Chem. Biol. 2018, 13, 2728−2738

compensated by other genes within the *ttn* cluster or the *S. griseochromogenes* genome under the conditions that were examined.[12] Subsequent efforts to directly characterize TtnD *in vitro* as a decarboxylase, however, met with mixed success: the recombinant TtnD enzyme, isolated from *E. coli* upon overexpression of the *ttnD* gene, could catalyze C-3″ decarboxylation of TTN D-1 to afford TTN I-1 as predicted, but at a very slow rate of 0.07 min^{-1} (Figure 3a).

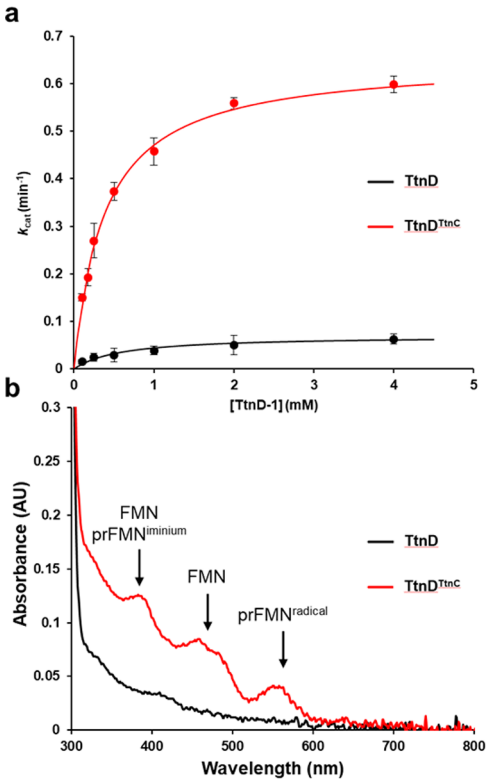

Figure 3. Enzymatic characterization of TtnD as a prFMN-containing decarboxylase. (a) Determination of the kinetic parameters for TtnD and TtnD^{TtnC} with TTN D-1 as a substrate. TtnD^{TtnC} (with an apparent k_{cat}/K_m value of 1.71 min^{-1} mM^{-1}) exhibited a catalytic efficiency significantly greater than that of TtnD (with an apparent k_{cat}/K_m value of 0.12 min^{-1} mM^{-1}), presumably because of the greater occupancy of prFMN in the active site of TtnD^{TtnC}. (b) UV−vis spectra of TtnD (black) and TtnD^{TtnC} (red). The three peaks seen in TtnD^{TtnC}, but not TtnD, clearly show the presence of prFMN[22] in TtnD^{TtnC}. Error bars represent standard deviations.

It was not until the recent findings of the UbiD family of decarboxylases, requiring a prFMN for their decarboxylase activity, and of the UbiX family of flavin prenyltransferases, synthesizing the novel prFNM cofactor from $FMNH_2$ and DMAP,[19−28] that we realized that TtnD might also require prFMN for its decarboxylase activity. The sequence of TtnD was significantly homologous to that of the UbiD family of decarboxylases, being 28 and 44% identical and 36 and 53% similar to those of UbiD and Fdc1, respectively (Figure S1). Upon searching the *ttn* cluster for homologues of the UbiX family of flavin prenyltransferases, we identified that the sequence of TtnC was 57 and 72% identical and 56 and 74% similar to those of UbiX and Pad1, respectively, serving as the candidate of the cognate flavin prenyltransferase for TtnD (Figure S2). Thus, we co-expressed *ttnD* with *ttnC* in *E. coli* to produce holo-TtnD (i.e., TtnD complexed with prFMN or TtnD^{TtnC}), with TtnD produced by expressing *ttnD* alone as a control (Figure S3). While the TtnD preparation was colorless, the TtnD^{TtnC} preparation was colored purple; during purification, however, we noticed a significant loss of the purple color from the TtnD^{TtnC} fractions between the immobilized metal affinity chromatography (IMAC) and size-exclusion steps, which was correlated with the loss of the non-covalently bound prFMN cofactor from holo-TtnD. To maximize the enzyme activity, we therefore decided to compromise the purity of the holo-TtnD by using the partially purified TtnD^{TtnC} fractions, after the IMAC step, in the current studies, which accounted for ∼51% TtnD purity (Figure S3).

We confirmed by liquid chromatography−mass spectrometry (LC−MS) analysis that co-expression of ttnD with ttnC in *E. coli*, followed by IMAC, indeed afforded holo-TtnD that contained a high prFMN content. The partially purified fraction of TtnD^{TtnC} (∼51% purity) was treated with CH_3CN to extract any non-covalently bound flavin cofactors, with a similarly prepared fraction of TtnD (∼59% purity) used as a control (Figure S3); the resultant CH_3CN extracts were subjected to LC−MS analysis. While no flavin cofactor was detected from TtnD, two major forms of prFMN were apparent from TtnD^{TtnC}, which were confirmed to be the prFMN^{iminium} and prFMN^{radical} species by high-resolution MS analysis (Figure S4).[19−22] These findings were further supported by direct comparison of the ultraviolet−visible (UV−vis) spectra between TtnD^{TtnC} and pure TtnD (Figure 3b and Figure S3). TtnD^{TtnC} exhibited distinct peaks at 387 and 550 nm, which are characteristic of the prFMN^{iminium} and prFMN^{radical} species, respectively; the peak at 458 nm indicated the presence of FMN,[22] which was also detected by LC−MS analysis of the CH_3CN extract made from TtnD^{TtnC} (Figure S4). In contrast, the spectrum of pure TtnD was completely devoid of any absorbance peaks in this wavelength range (Figure 3b). Taken together, these results support TtnC being a member of the UbiX family of flavin prenyltransferases, in which co-expression of *ttnD* allows the production of TtnD in its holo form.

TtnD^{TtnC} as a Competent Decarboxylase. We performed *in vitro* assays of TtnD^{TtnC}, with TtnD as a control, and demonstrated TtnD^{TtnC} as a decarboxylase that is much more efficient than TtnD in catalyzing C-3″ decarboxylation of TTN D-1 to afford TTN I-1 *in vitro*. TTN D-1, isolated from Δ*ttnD* mutant SB13013,[11] was used as the substrate for the *in vitro* assays, with TTN I-1 isolated from Δ*ttnI* mutant SB13017[12] as the authentic standard of the product for high-performance liquid chromatography (HPLC) and LC−MS analysis (Figure S5). Under the optimized assay conditions, TtnD^{TtnC} exhibited an optimal activity at pH 6.5 (Figure S6), catalyzing efficient C-3″ decarboxylation of TTN D-1 to afford TTN I-1, the identity of which was confirmed by HPLC and LC−MS analysis in comparison with the authentic standard of TTN I-1; no activity was detected with the control assay using boiled TtnD^{TtnC} (Figure S7a). The steady-state kinetic parameters for the TtnD^{TtnC}-catalyzed decarboxylation of TTN D-1 were then determined, in comparison with those of TtnD (Figure 3a). The formation of TTN I-1 by both TtnD^{TtnC} and TtnD followed Michaelis−Menten kinetics, with an apparent K_m value of 0.38 ± 0.03 mM and an apparent k_{cat} value of 0.65 ± 0.01 min^{-1} for TtnD^{TtnC} and with an apparent K_m value of 0.58 ± 0.23 mM and an apparent k_{cat} value of 0.07 ± 0.01 min^{-1} for TtnD (Figure 3a) (apparent kinetic parameters were used because of the uncertainty of the prFMN^{iminium} content and the

DOI: 10.1021/acschembio.8b00673
ACS Chem. Biol. 2018, 13, 2728−2738

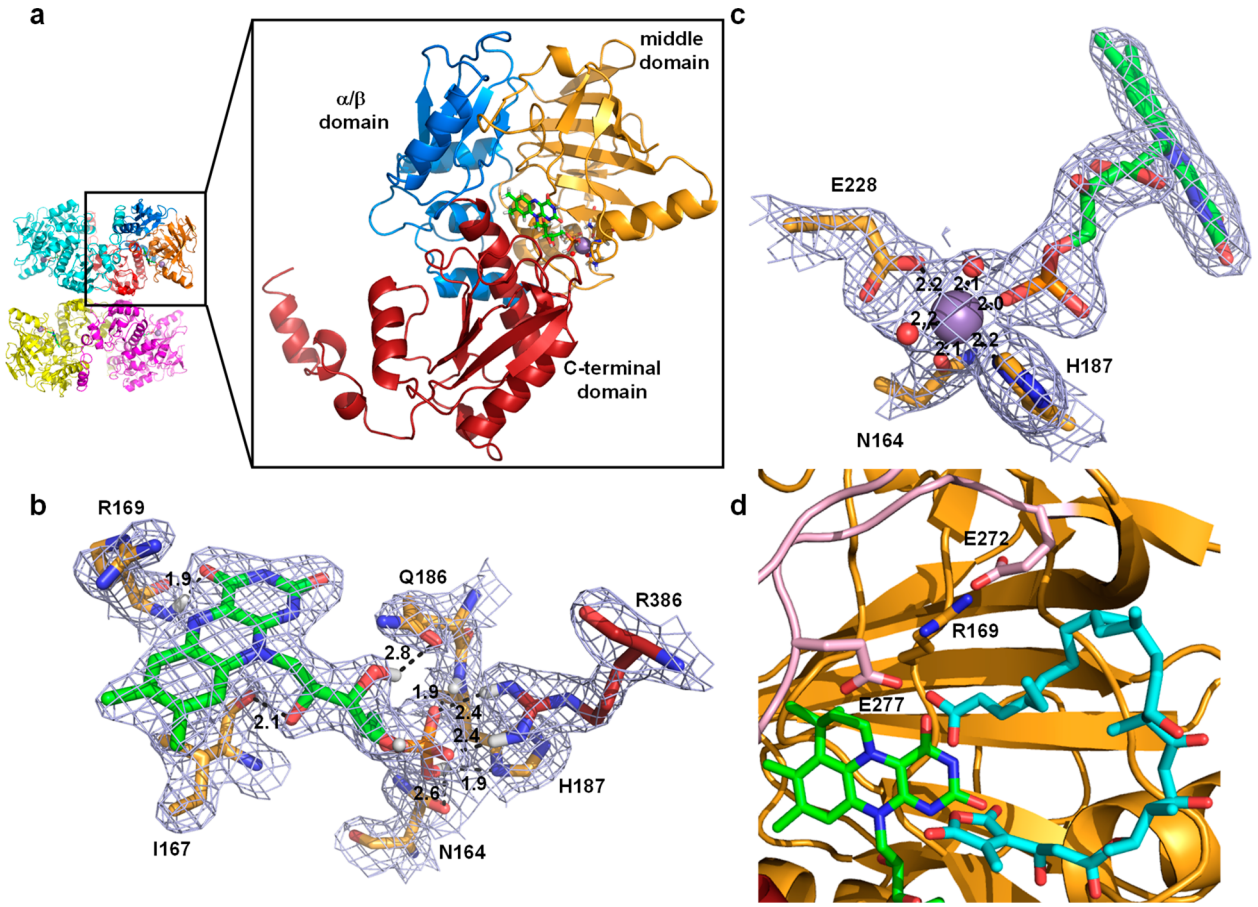

Figure 4. Structure of TtnD revealing a similar UbiD-like fold of the UbiD family of carboxylases.[14−16,19,22,29,30] (a) The overall structure of TtnD is a homotetramer. Each protomer is composed of three domains: α/β domain, middle domain, and C-terminal domain colored blue, orange, and red, respectively. FMN (green) is located between the middle domain and C-terminal domains. Mn(II) and H_2O are shown as purple and red spheres, respectively. (b) FMN forms hydrogen bonds with N164, I167, R169, Q186, H187, and R386. (c) Mn(II) is bound in an octahedral coordination geometry and binds the phosphate of FMN in the FMN binding pocket. (d) A loop missing in the structure of TtnD was modeled using I-TASSER[32−34] (pink). prFMN (green) and TTN D-1 (light blue) were docked using AutoDock4.[35] The E272-E277-R169 catalytic triad forms a salt bridge network. The carboxylic acid and adjacent double bond of TTN D-1 are positioned in the proximity of prFMN. E277 is pointing toward the double bond of TTN D-1.

estimated purity of TtnD during $TtnD^{TtnC}$ preparation). $TtnD^{TtnC}$ (with an apparent k_{cat}/K_m value of 1.71 min^{-1} mM^{-1}) exhibited a catalytic efficiency 14.25-fold greater than that of TtnD (with an apparent k_{cat}/K_m value of 0.12 min^{-1} mM^{-1}), presumably because of the greater occupancy of prFMN in the active site of $TtnD^{TtnC}$. We attributed the residual activity from TtnD, when overproduced in *E. coli* in the absence of TtnC, to the trace amount of prFMN provided by the *E. coli* host. This would be consistent with the finding that Δ*ttnC* mutant SB13012 retained the full competency in TTN production,[12] the TtnC function of which must have been complemented by another flavin prenyltransferase encoded within the *S. griseochromogenes* genome.

$TtnD^{TtnC}$ showed significant substrate promiscuity, decarboxylating a variety of TTN analogues, but did not decarboxylate non-polyketide substrates. Inspired by the fact that Fdc1 exhibited broad substrate promiscuity toward substituted cinnamic acids,[18−20] we first tested if $TtnD^{TtnC}$ could catalyze the decarboxylation of cinnamic acid. No activity was detected under any conditions tested (Figure S7b), revealing a distinct substrate specificity between TtnD and Fdc1 (also see Figure 5). We next took advantage of TTN D-2, TTN D-3, and TTN D-4, three structural analogues of TTN D-1 isolated from Δ*ttnD* mutant SB13013 that all featured the same α,β-unsaturated acid moiety but with varying substitutions at C-5,[11] as well as TTN F-1, the structural analogue of TTN D-1 isolated from Δ*ttnF* mutant SB13014 that lacked the α,β-double bond conjugated to the C-3″ carboxylic acid[11] (Figure 1), as alternative substrates and asked if they could be decarboxylated by $TtnD^{TtnC}$. $TtnD^{TtnC}$-catalyzed C-3″ decarboxylation was readily detected for TTN D-2, TTN D-3, and TTN D-4, with the identity of the corresponding terminal alkene products confirmed by LC−MS analysis; no activity was detected with the control assays using boiled $TtnD^{TtnC}$ (Figure S7c−e). In comparison with TTN D-1, $TtnD^{TtnC}$ exhibited 16, 64, and 11% relative activity with TTN D-2, TTN D-3, and TTN D-4, respectively, as an alternative substrate. These findings are consistent with our previous proposal for TTN biosynthesis,[12] supporting TTN D-1 as the native substrate of TtnD (Figure 1). In contrast, no activity was detected for TTN F-1 under the same assay condition (Figure S7f), a finding that supports the necessity of the α,β-double bond conjugated to the C-3″ carboxylic acid for TtnD catalysis, specifically the formation of the prFMN−substrate adduct via the proposed [3+2] cycloaddition[19−28] (Figure 2c).

DOI: 10.1021/acschembio.8b00673
ACS Chem. Biol. 2018, 13, 2728−2738

TtnD Structure Revealing a UbiD-like Fold. To obtain insight into the catalytic mechanism of TtnD, the X-ray structures of TtnD, in the apo form (i.e., $TtnD^{apo}$) and in complex with FMN (i.e., $TtnD^{FMN}$), were determined. TtnD shares a similar UbiD-like fold with the other members of the UbiD family of decarboxylases.[14−16,19,22,29,30] Unfortunately, we were unable to obtain TtnD with bound prFMN; instead, we co-crystallized TtnD with FMN as a surrogate for the holo form (i.e., $TtnD^{FMN}$). Crystals of $TtnD^{apo}$ [Protein Data Bank (PDB) entries 6DA6 and 6DA7] belong to orthorhombic space group $P2_12_12_1$ with unit cell dimensions of a = 53.22 Å, b = 137.12 Å, and c = 284.07 Å and to orthorhombic space group $I222$ with unit cell dimensions of a = 52.35 Å, b = 114.39 Å, and c = 194.35 Å. Crystals of $TtnD^{FMN}$ (PDB entry 6DA9) belong to orthorhombic space group $I222$ with unit cell dimensions of a = 52.07 Å, b = 116.11 Å, and c = 193.97 Å. The crystal structures were determined by molecular replacement using the structure of PA0254 (PDB entry 4IWS)[29] as a model. The final models were refined to resolutions of 2.59, 1.83, and 2.05 Å for the 6DA6, 6DA7, and 6DA9 structures, respectively (Table S1).

The $TtnD^{apo}$ (PDB entry 6DA7) and $TtnD^{FMN}$ structures show a high degree of structural similarity and exhibit a root-mean-square deviation (RMSD) of 0.15 Å over 388 Cα atoms, suggesting that the binding of flavin does not induce any significant conformational changes (Figure S8a). TtnD forms a homotetramer, i.e., a dimer of dimers (Figure 4a), which agrees well with its tetrameric structure in solution as determined by side-exclusion chromatography (Figure S9). Each protomer consists of three domains (Figure 4a). The N-terminal α/β domain (M1−R105 and D301−V314) consists of four-stranded mixed β-sheets, flanked by α-helices on both sides. The N-terminal domain interacts with the two other domains and forms one lobe of the bilobal protomer protein. Electron density for part of the N-terminal α/β domain (P266−Q289) is missing, suggesting that this loop is flexible without TTN D-1 bound. The middle domain (E106−R300) is formed by a six-stranded antiparallel β-sheet wrapped by α-helices and β-strands. The C-terminal domain (D315−A485) forms the second lobe of the protomer; a long α-helix links the two lobes. The core of the C-terminal domain is a central five-stranded β-sheet flanked by three α-helices. The C-terminal tail (A460−A485) from one protomer binds with a neighboring protomer. The interactions between protomers are mainly mediated through the C-terminal domains. The interactions between protomers A and C involve helix α14, which packs against the β-sheet of the C-terminal domain from the second protomer. Additional interactions are formed by C-terminal helix α16, which interacts with the N-terminal and middle domains of the neighboring protomer. The interactions between dimers AC and BD are mediated by helix α13 of the C-terminal domain, which packs against β-sheets in the C-terminal domain of the neighboring protomer. PISA analysis of the TtnD structure reveals that the tetrameric structure is stabilized by multiple hydrogen bonds and ionic interactions; the buried interface areas between subunits A and C and dimers AC and BD were calculated to be 2882 and 1699 $Å^2$, respectively. The total interface area of each protomer that becomes buried upon assembly is 3732 $Å^2$ (Figure S10).[31]

The overall structure of TtnD is highly similar to those of UbiD from *E. coli* (RMSD = 2.54 Å over 333 Cα atoms),[22] Fdc1 from *A. niger* (RMSD = 2.27 Å over 325 Cα atoms), *Saccharomyces cerevisiae* (RMSD = 1.26 Å over 364 Cα atoms), and *Candida dubliniensis* (RMSD = 1.04 Å over 312 Cα atoms),[19] PA0254 from *Pseudomonas aeruginosa* (RMSD = 1.31 Å over 377 Cα atoms),[29] and AroY from *Klebsiella pneumoniae* (RMSD = 2.21 Å over 289 Cα atoms) and *Enterobacter cloacae* (RMSD = 1.67 Å over 278 Cα atoms) (Figure S11a).[30] The missing residues (P266−Q289) within the N-terminal α/β domain of TtnD form two antiparallel β-sheets linked by a loop (Figure S11b). This structure extends from the top of the middle domain to near the FMN/Mn(II) binding pocket and putative TTN D-1 binding site of TtnD. The binding pocket for prFMN is located in the cleft between the middle domain and the C-terminal domain. Superposition of the TtnD−FMN complex structure with the *A. niger* Fdc1−prFMN complex structure (PDB entry 4ZA4) shows that TtnD binds FMN in a mode identical to that in which Fdc1 binds prFMN (Figure S11). FMN forms hydrogen bonds with several residues in TtnD. R169 binds to the isoalloxazine ring; I167 and Q186 bind to the ribityl chain, and N164, H187, and R386 bind to the phosphate group (Figure 4b). R169 is highly conserved in the UbiD family of decarboxylases; the other residues are either predominantly conserved or semiconserved (Figure S1). A Mn(II) ion is bound with an octahedral coordination geometry with respect to the side chains of N164, H187, and a highly conserved E228, an oxygen of the phosphate group of FMN, and a water molecule (Figure 4c and Figure S2). Furthermore, two distinct active site conformations have been described for the UbiD family of decarboxylases: "open" for AroY and UbiD and "closed" for Fdc1.[22,30] Superposition of the whole chain, the N-terminal domain, or the C-terminal domain of TtnD with Fdc1 suggests that the active sites share the same closed conformation (Figure S11). Moreover, different protomers from a multimeric protein do not necessarily have the same conformation, like those seen in UbiD that have different degrees of an open conformation.[22] Structure alignments of the four protomers of TtnD using the whole chain, the N-terminal domain, or the C-terminal domain verify that they all share the same conformation (Figure S8b).

Substrate Docking Supporting the Catalytic Triad of TtnD. The missing part (P266−Q289) within the N-terminal α/β domain of the determined $TtnD^{apo}$ and $TtnD^{FMN}$ structures contains E272 and E277, the two conserved residues that likely play a key role in TtnD catalysis.[14−16] Given that they share the same active site conformation, we first rebuilt the missing part into the TtnD structure using the Fdc1 structure as a model[19] and subsequently docked prFMN and TTN D-1 to the complete model of TtnD (Figure 4d).[32−35] prFMN is bound in a manner identical to that of FMN in the $TtnD^{FMN}$ structure. TTN D-1 is located in a horseshoe-like conformation in the active site with the dialkylmaleic anhydride moiety and the carboxylic acid facing inward toward the active site with the polyketide chain of the substrate facing away. The dialkylmaleic anhydride forms hydrogen bonds with the side chains of Q186 and N431, and the carboxylic acid makes a hydrogen bond with the side chain of R169 (Figure 4d). C-1″ and C-2″ of TTN D-1 are in the proximity of C-1′ and C-4a of prFMN, a necessary orientation for the proposed [3+2] cycloaddition in TtnD catalysis (also see Figure 2c). As in the Fdc1 structure,[19] the R169-E272-E277 catalytic triad forms a salt bridge network with E277 pointing toward C-2″ of TTN D-1, which allows acid catalysis to release the alkene product via the proposed retro-[3+2] cyclo-elimination between prFMN and TTN D-1 (Figure 2c). This model

DOI: 10.1021/acschembio.8b00673
ACS Chem. Biol. 2018, 13, 2728−2738

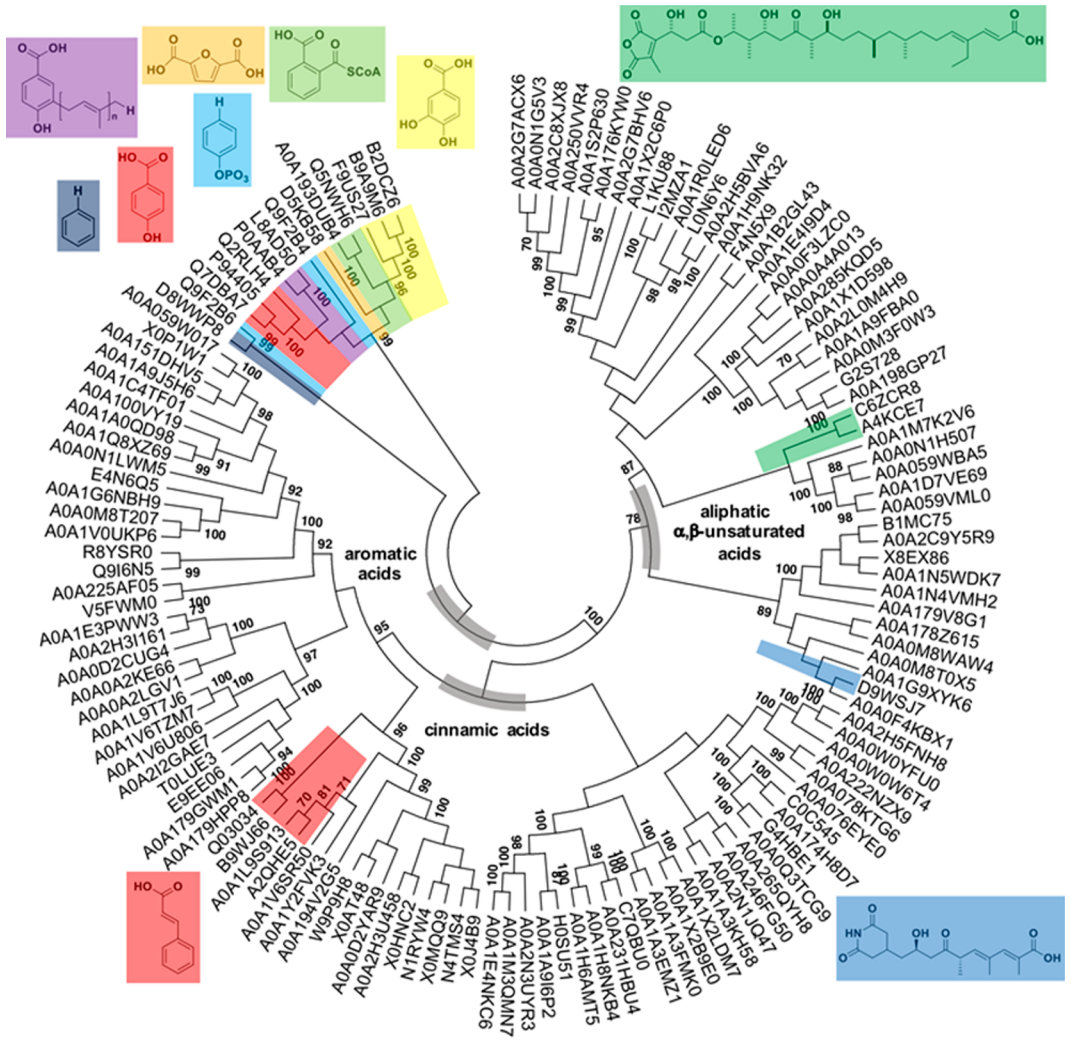

Figure 5. Phylogenetic tree of the characterized TtnD homologues and the 112 selected TtnD homologues that are clustered with TtnC homologues (Table S2). The sequence alignment and phylogenetic tree were made with ClustalW and the neighbor-joining method in MEGA, respectively.[38,40] The TtnD homologues fall into three distinct clades: the UbiD clade naturally acts on aromatic acids, the Fdc1 clade naturally acts on cinnamic acids, and the TtnD clade naturally acts on aliphatic α,β-unsaturated acids (also see Figure 2). Members from each clade whose substrates have been predicted bioinformatically or confirmed experimentally are color-coded and highlighted with their respective substrates shown. While the structure of PA0254 (UniProtKB entry Q9I6N5) has been determined, its natural substrate remains unestablished.[29]

agrees well with the observed substrate promiscuity of TtnD, the substrate binding pocket of which could readily accommodate TTN D-2, TTN D-3, and TTN D-4, in a fashion similar to that of TTN D-1, but differentiate cinnamic acid because of its lack of key interactions with the dialkylmaleic anhydride moiety (Figure 4d).

Mutational Analysis Confirming TtnD Catalysis. The structures of $TtnD^{apo}$ and $TtnD^{FMN}$, together with the rebuilt TtnD structure, docked with TTN D-1 and prFMN, clearly revealed that R169, E272, and E277 constitute the catalytic triad for TtnD and E228 plays a critical role in prFMN binding (Figure 4). To provide additional experimental data to support their roles in prFMN binding and TtnD catalysis, each of these four residues was individually mutated to alanine by site-directed mutagenesis to generate the corresponding R169A, E272A, E277A, and E228A mutants of TtnD. These mutants were similarly overproduced in and partially purified from *E. coli* in the presence of TtnC, with wild-type $TtnD^{TtnC}$ as a control (Figure S3), and tested for their decarboxylase activity using TTN D-1 as the substrate. Their prFMN contents were similarly determined by comparing their UV−vis spectra (Figure S12a) and analyzing their extractable noncovalently bound flavin cofactors by LC−MS (Figure S12b). These results revealed that each of the mutants completely abolished their enzymatic activity, indicating that these residues are essential for TtnD-catalyzed C-3″ decarboxylation of TTN D-1. Intriguingly, while the E228A mutant nearly lost all of its ability to bind flavin, as expected because E228 was predicted to play a key role in prFMN binding, all four mutants completely abolished their ability to bind prFMN (either the $prFMN^{iminium}$ or $prFMN^{radical}$ form), with the R169A and E272A mutants exhibiting significant binding to FMN instead (Figure S12). These results suggest that R169 and E272 may also contribute to selective binding of prFMN. Finally, the E277A mutant, like TtnD produced in the absence of TtnC, is completely devoid of any flavin cofactor (Figure S12). E277 therefore, in addition to playing a catalytic role, may also be involved in prFMN formation and binding, though these mutational studies fell short of defining the exact role TtnD may play in the TtnC-catalyzed biosynthesis of prFMN and its

DOI: 10.1021/acschembio.8b00673
ACS Chem. Biol. 2018, 13, 2728−2738

subsequent oxidation into the active form, prFMN^{iminium} (Figure 2b).

UbiD Family Subtypes Correlating to Substrates. Members of the UbiD family of decarboxylases are widely distributed in archaeal, bacterial, and fungal genomes.[15,29,36] Among the ones that have been biochemically characterized to date, they catalyze decarboxylation of either aromatic acids, as exemplified by UbiD[22] or AroY,[30] or substituted cinnamic acids, as exemplified by Fdc1[19] (Figure 2). It should be noted that every enzyme has different degrees of substrate promiscuity. For example, the natural substrate of Fdc1 is cinnamic acid, but Fdc1 also accepts aliphatic compounds, including sorbic acid as a substrate.[37] The discovery of prFMN as a novel cofactor for the UbiD family of decarboxylases in general and mechanistic and structural characterization of Fdc1 in specific has unveiled a mechanism involving an unprecedented biological [3+2] cycloaddition between prFMN^{iminium} and the double bond of the α,β-unsaturated acid substrate for this family of enzymes.[14−16] While this mechanism is consistent with all the experimental evidence for Fdc1,[19−28] generalization of the same mechanism to members of the UbiD family that act on aromatic acids would require prFMN^{iminium} to react directly with the benzene ring of the substrates, thereby invoking a significant energetic barrier due to the loss of aromaticity.[25] In fact, a recent study of AroY, which catalyzes decarboxylation of 3,4-dihydroxybenzoic acid, has provided the strongest evidence yet supporting an alternative mechanism, involving a quinoid intermediate.[30] Taken together, these results have raised the question of whether Fdc1 is a mechanistic outlier or whether there are other members of the UbiD family that share the same [3+2] cycloaddition mechanism as Fdc1.[25] TtnD represents the first example of the UbiD family of carboxylases that naturally acts on an aliphatic α,β-unsaturated acid.[14−16] Comparative studies of the structure and active site between TtnD and Fdc1 clearly support the idea that TtnD catalyzes decarboxylation of TTN D-1 proceeding by the same [3+2] cycloaddition mechanism as Fdc1 (Figure 2). TtnD therefore supports the [3+2] cycloaddition mechanism and expands the substrate scope, beyond aromatic and cinnamic acids, for the UbiD family of carboxylases.

Previous bioinformatics analysis of the UbiD family of carboxylases has been primarily based on UbiD and its homologues.[15,19,36] With TtnD as a new member of the UbiD family of decarboxylases, we performed additional bioinformatics analysis, centering on TtnD and taking its clustering with TtnC encoded within the same biosynthetic gene cluster[9,10] into consideration. Using the Enzyme Function Initiative-Genome Neighborhood Network Tool (EFI-GNT),[38] we searched the public databases for TtnD homologues and identified 200 homologues of which 112 homologues had TtnC-like homologues encoded in the genetic proximity (Table S2). These homologues, with sequences that are 21−99% identical, including the 21 TtnD homologues whose functions have been either confirmed biochemically or predicted bioinformatically or whose structures have been determined, were used to build a phylogenetic tree. Remarkably, the homologues fall into three distinct clades, each of which is represented by the characterized members that naturally act on the three different types of substrates, i.e., aromatic acids, cinnamic acids, and aliphatic α,β-unsaturated acids (Figure 5).

The findings gleaned from the bioinformatics analysis could have multiple ramifications for the chemistry and enzymology of the UbiD family of decarboxylases. First, sequences according to the three distinct clades could be used to predict substrate types. This is further supported by the structures of the four enzymes determined to date. UbiD[22] and AroY,[30] both acting on aromatic acids, are hexameric. Fdc1,[19] acting on its natural substrate, cinnamic acid, is dimeric. TtnD in this study, acting on aliphatic α,β-unsaturated acids, is tetrameric. PA0254,[29] the function of which has not been demonstrated biochemically, falls into the same clade as Fdc1 and is also dimeric. Second, the substrate scope for the UbiD family of enzymes is much broader than is currently appreciated.[14−16] While the UbiD family of enzymes has been most known as decarboxylases that act on aromatic acids, Fdc1, TtnD, and homologues have clearly emerged as two distinct subtypes that act on varying substrate types beyond aromatic acids. Third, biological [3+2] cycloaddition, first discovered as an unprecedented mechanism for Fdc1 catalysis,[19] is apparently more common than previously thought because of the wide distribution of Fdc1 and TtnD homologues in nature. Characterization of new members of the Fdc1 and TtnD subtypes or a search for new subtypes, distinct from UbiD, Fdc1, and TtnD, promises to further extend prFMN-associated catalysis and enzymology. Finally, the growing substrate scope and catalytic repertoire for the UbiD family of decarboxylases will surely inspire further exploitation of these enzymes as biocatalysts for the production of aliphatic terminal alkenes from α,β-unsaturated acids.[39] Because these enzymes catalyze reversible decarboxylation, they could also be exploited as biocatalysts, utilizing CO_2 as an abundant carbon source, for sustainable chemical production.[30]

METHODS

General Method. DNA amplification and mutagenesis were performed with a model S1000 thermal cycler (Bio-Rad). The proteins were purified on an ÄKTA Pure instrument (GE Healthcare Life Sciences). UV−vis spectra were recorded with a NanoDrop 2000C spectrophotometer (Thermo Scientific). LC−MS analysis was performed on an Agilent 1260 Infinity LC instrument coupled to a 6230 TOF instrument (HRESI) equipped with an Agilent Poroshell 120 EC-C18 column (50 mm × 4.6 mm, 2.7 μm). HPLC was performed on an Agilent 1260 Infinity II instrument equipped with an Agilent Zorbax SB-C18 column (150 mm × 4.6 mm, 5 μm).

Gene Cloning. The *ttnD* and *ttnC* genes were amplified by polymerase chain reaction from the genomic DNA of *S. griseochromogenes* using the TtnD-F, TtnD-R, TtnC-F, and TtnC-R primers and Phusion HF DNA polymerase (NEB) following the protocol provided by the manufacturer (Table S3). The amplified *ttnD* sequence was cloned into the *Eco*RI and *Hin*dIII sites of pCDFDuet-1 (Novagen) to give pBS13033. The amplified *ttnC* sequence was cloned into pBS13033 at the *Nde*I and *Kpn*I sites to give pBS13034. The R169A, E228A, E272A, and E277A mutants of TtnD were obtained by site-directed mutagenesis using Phusion HF DNA polymerase, pBS13034 as the template, and the R169A-F, R169A-R, E228A-F, E228A-R, E272A-F, E272A-R, E277A-F, and E277A-R primers to give pBS13035, pBS13036, pBS13037, and pBS13038, respectively (Tables S3 and S4).

Protein Production and Purification. Each of the expression constructs was transformed into *E. coli* BL21 (DE3). The resultant recombinant strains were grown in lysogeny broth supplemented with 1 mM $MnCl_2$ at 37 °C until an OD_{600} of 0.6 was reached. The cells were cooled to 4 °C; the expression of the targeted genes was induced by addition of 0.1 mM isopropyl β-D-1-thiogalactopyranoside, and the cells were grown at 18 °C for 16 h. The cells were harvested at 4000*g* for 15 min at 4 °C, and the pellet was resuspended in lysis buffer [100

DOI: 10.1021/acschembio.8b00673
ACS Chem. Biol. 2018, 13, 2728−2738

mM Tris (pH 8.0) containing 300 mM NaCl, 15 mM imidazole, and 10% glycerol]. After sonication, the cell debris was removed by centrifugation at 15000*g* for 15 min at 4 °C. The lysate was loaded onto a HisTrap 5 mL column (GE) equilibrated with washing buffer [50 mM Tris (pH 8.0) containing 100 mM NaCl and 15 mM imidazole]. The column was washed with washing buffer, and the His_6-tagged protein was eluted using elution buffer [50 mM Tris (pH 8.0) containing 100 mM NaCl and 300 mM imidazole]. Following elution, the protein was desalted using a PD-10 desalting column (GE) in 50 mM Tris buffer (pH 8.0) containing 100 mM NaCl and stored at −80 °C. To obtain pure TtnD, the protein, from co-expression of *ttnD* with *ttnC*, as well as expression of *ttnD* alone, was injected onto a Superdex S200 16/600 gel filtration column (GF) after IMAC using 50 mM Tris buffer (pH 8.0) containing 100 mM NaCl and stored at −80 °C.

Isolation of TTN Analogues. According to previously reported procedures, TTN D-1, TTN D-2, TTN D-3, and TTN D-4 were isolated from Δ*ttnD* mutant SB13013,[11] TTN F-1 was isolated from Δ*ttnF* mutant SB13014,[11] and TTN I-1 was isolated from Δ*ttnI* mutant SB13017.[12]

TtnD Activity Assays. Preliminary reactions were performed in 50 mM Tris (pH 8.0) containing 100 mM NaCl and 1 mM $MnCl_2$ in a total volume of 50 μL. After incubation at 28 °C in the dark for 1 h, 50 μL of acetonitrile was added to quench the reaction. After centrifugation, 10 μL was injected and analyzed by LC−MS with UV detection at 230 nm. The mobile phase was composed of buffer A (H_2O containing 0.1% acetic acid) and buffer B (CH_3CN containing 0.1% acetic acid). A linear gradient from 5 to 100% buffer B for 18 min and then 100% buffer B for 7 min was used with re-equilibration to 95% buffer A for 5 min using a flow rate of 0.4 mL min^{-1}.

To determine the pH dependence of TtnD, reactions of 400 μM TTN D-1, 1 mM $MnCl_2$, and 28 μM TtnD in various buffers with pHs ranging from 5.5 to 9.0 were performed in volumes of 25 μL and mixtures incubated for 1 h at 28 °C in the dark. The following buffers were tested: 50 mM MES and 100 mM NaCl at pH 5.5 and 6.0; 50 mM phosphate and 100 mM NaCl at pH 6.0, 6.5, 7.0, 7.5, and 8.0; and 50 mM Tris and 100 mM NaCl at pH 8.0, 8.5, and 9.0. Each reaction was quenched by the addition of 25 μL of acetonitrile. After centrifugation, 10 μL was injected and analyzed by HPLC with UV detection at 230 nm. The mobile phase was composed of buffer A (H_2O containing 0.1% acetic acid) and buffer B (CH_3CN containing 0.1% acetic acid). A linear gradient from 5 to 80% buffer B for 3 min and a linear gradient from 80 to 100% buffer B for 5 min, and then 100% buffer B for 5 min, was used with reequilibration to 95% buffer A for 3 min using a flow rate of 0.8 mL min^{-1}. The areas of the peaks corresponding to TTN I-1 were integrated, and the concentrations of the product were obtained using the calibration curve of the TTN I-1 standard (Figure S5).

Initial rate measurements for the determination of kinetic parameters were taken in 50 mM phosphate buffer (pH 6.5) containing 1 mM $MnCl_2$ at various TTN D-1 concentrations (0.1, 0.175, 0.25, 0.5, 1, 2, and 4 mM) over 1 h at 28 °C in the dark. The reactions were quenched and analyzed by HPLC as described above. The data were fit to the Michaelis−Menten equation using nonlinear regression analysis using GraphPad Prism.

For the evaluation of substrate promiscuity, each substrate (TTN D-2, TTN D-3, TTN D-4, TTN F-1, or cinnamic acid) at 400 μM was mixed with 1 mM $MnCl_2$ and 28 μM TtnD in 50 mM phosphate buffer (pH 6.5) for 1 h at 28 °C in the dark. Each reaction was quenched and analyzed by LC−MS as described above. The resulting enzymatic products were analyzed by negative mode ionization and UV detection at 230 nm. The activity of TtnD with the different substrates was estimated by the consumption of the substrates compared to the reaction with TTN D-1.

Extraction of Flavin Cofactors. One hundred microliters of 60 μM protein was mixed with an equal volume of CH_3CN and heated at 70 °C for 5 min. After elimination of the precipitants by centrifugation, 10 μL was injected and analyzed by LC−MS using the method described above.

Spectroscopic Analysis. The UV−vis spectrum of each protein, at a concentration of 50 μM in 50 mM Tris buffer (pH 8.0) containing 100 mM NaCl, was measured between 300 and 800 nm. The same buffer was used as a blank.

Crystallization of TtnD. TtnD, at a concentration of 18.6 mg mL^{-1} in buffer containing 10 mM tetraethylammonium hydroxide (TEAOH) (pH 7.5), 20 mM NaCl, and 10 mM KCl, was mixed with a reservoir solution in a 1:1 to 1:1.5 volume ratio in a sitting drop crystallization trial. Multiple initial hits were obtained from the Morpheus HT broad screen or the Midas (Molecular Dimensions, Inc.) alternative polymer screen. The *I*222 $TtnD^{apo}$ crystals were optimized around condition E4 of the Midas screen using a reservoir solution of 40% (v/v) pentaerythritol propoxylate (5/4 PO/OH), 0.10 M HEPES [4-(2-hydroxyethyl)-1-piperazineethanesulfonic acid (pH 7.0)], and 0.20 M sodium thiocyanate (PDB entries 6DA7 and 6DA9). $P2_12_12_1$ crystals were optimized around condition A3 of the Morpheus screen with a reservoir solution of 10% (w/v) polyethylene glycol 4000, 0.062 M MES [2-(*N*-morpholino)ethanesulfonic acid (pH 6.5)], 0.038 M imidazole (pH 6.5), 0.03 M calcium chloride, 0.03 M magnesium chloride, and 20% (v/v) glycerol (PDB entry 6DA6). The *I*222 $TtnD^{apo}$ crystals were cryoprotected with an artificial mother liquor containing 20% glycerol in the precipitant solution and flash-cooled in liquid nitrogen. FMN complex crystals were obtained by soaking *I*222 $TtnD^{apo}$ crystals in a precipitant solution with 3 mM TtnD1, 3 mM $MnCl_2$, 0.5 mM FMN, and 20% glycerol. Colorless crystals turned yellow immediately after being soaked.

Data Collection, Structure Determination, and Refinement. Diffraction data were collected at the Advanced Photon Source (Argonne, IL) at the General Medical Sciences and Cancer Institute's Structural Biology Facility on Advanced Photon Source (GM/CA @ APS) beamlines 23-ID-B and 23-ID-D, Life Sciences Collaborative Access Team (LS-CAT) beamlines 21-ID-D, 21-ID-F, and 21-ID-G, and Lilly Research Laboratories Collaborative Access Team (LRL-CAT) beamline 31-ID. The TtnD data sets were indexed, reduced, and scaled with *XDS*.[41] Initial phases for the $P2_12_12_1$ apo crystal were obtained by molecular replacement with *phaser* from the Phenix suite[42] using domains from PDB entry 4IWS (PA0254 from *P. aeruginosa*)[29] as search models. Structural models were rebuilt and refined with *Coot*,[43] *phenix.refine*,[44] and *Buster-TNT*[45] with a collaborative visualization tool.[46] The refinement model included four TLS groups per protomer. For the lower-resolution FMN and $P2_12_12_1$ apo structures, additional target restraints to the higher-resolution apo structure were included along with noncrystallographic symmetry (NCS) restraints for the $P2_12_12_1$ apo structure.[47] Electron density is weak for portions of two of the four chains in the asymmetric unit of the $P2_12_12_1$ apo structure, and these regions were modeled on the basis of the target and NCS restraints. The stereochemistry of the structure was checked with PROCHECK and MolProbity.[48,49] Data collection and refinement statistics are listed in Table S1.

The atomic coordinates and experimental structure factors of TtnD were deposited in the PDB as entries 6DA6 and 6DA7 ($P2_12_12_1$ and *I*222 $TtnD^{apo}$, respectively) and 6DA9 (*I*222 $TtnD^{FMN}$).

Substrate Docking. The missing loop in the structure of TtnD (PDB entry 6DA9) was modeled using I-TASSER.[32−34] The resulting protein model was used to perform the docking of TTN D-1 using Autodock4.[35]

Phylogenetic Analysis of TtnD Homologues. Amino acid sequences of the TtnD homologues were collected using the EFI-GNT.[38] From the 200 homologues, 112 sequences clustered with TtnC homologues encoded in the genetic proximity. From these 112 homologues and the 21 characterized TtnD homologues, a bootstrap consensus tree was generated by MEGA using the neighbor-joining method with a bootstrap test of 1000 replicates.[40]

DOI: 10.1021/acschembio.8b00673
ACS Chem. Biol. 2018, 13, 2728−2738

■ ASSOCIATED CONTENT

Supporting Information

The Supporting Information is available free of charge on the ACS Publications website at DOI: 10.1021/acschembio.8b00673.

Crystal parameters and data collection and refinement statistics (Table S1), a list of the TtnD homologues for phylogenetic analysis (Table S2), primers and the plasmids used in this study (Table S3), sequence alignment of TtnD with characterized members of the UbiD family (Figure S1), sequence alignment of TtnC with Pad1 and UbiX (Figure S2), sodium dodecyl sulfate−polyacrylamide gel electrophoresis analysis of the proteins used in this study (Figure S3), analysis of the cofactors from $TtnD^{TtnC}$ and TtnD (Figure S4), calibration curve for TTN I-1 (Figure S5), determination of the optimal pH for TtnD (Figure S6), *in vitro* assays of $TtnD^{TtnC}$ (Figure S7), superposition of the TtnD protomers (Figure S8), determination of the molecular weight of TtnD by size-exclusion chromatography (Figure S9), structure of tetrameric TtnD (Figure S10), superposition of TtnD and Fdc1 protomers (Figure S11), and analysis of the cofactor from the $TtnD^{TtnC}$ mutants (Figure S12) (PDF)

■ AUTHOR INFORMATION

Corresponding Author

*E-mail: shenb@scripps.edu.

ORCID

Jeffrey D. Rudolf: 0000-0003-2718-9651

Dong Yang: 0000-0003-2917-0663

Ben Shen: 0000-0002-9750-5982

Present Addresses

#G.X.: School of Life Science and Technology, University of Electronic Science and Technology of China, Chengdu 610054, China.

@M.M.: State Key Laboratory of Natural and Biomimetic Drugs, School of Pharmaceutical Sciences, Peking University, Beijing, China 100191.

Funding

This work is supported in part by National Institutes of Health Grants GM098248 (to G.N.P.), CA078747 (to B.S.), and GM115575 (to B.S.) and National Science Foundation BioXFEL STC Grant 1231306 (to G.N.P.). This research used resources of the Advanced Photon Source, a U.S. Department of Energy (DOE) Office of Science User Facility operated for the DOE Office of Science by Argonne National Laboratory under Contract DE-AC02-06CH11357. The use of Structural Biology Center beamlines at the Advanced Photon Source was supported in part by the DOE Office of Biological and Environmental Research, under Contract DE-AC02-06CH113. Use of the Lilly Research Laboratories Collaborative Access Team (LRL-CAT) beamline at Sector 31 of the Advanced Photon Source was provided by Eli Lilly Co., which operates the facility. GM/CA@APS has been funded in whole or in part with Federal funds from the National Cancer Institute (ACB-12002) and the National Institute of General Medical Sciences (AGM-12006). Use of LS-CAT Sector 21 was supported by the Michigan Economic Development Corp. and the Michigan Technology Tri-Corridor (Grant 085P1000817). J.D.R., C.-Y.C., and I.C. are supported in part by an Arnold O. Beckman Postdoctoral Fellowship, the Fellowship of Academia Sinica-The Scripps Research Institute Postdoctoral Talent Development Program, and the German Research Foundation (DFG) postdoctoral fellowship, respectively.

Notes

The authors declare no competing financial interest.

■ ACKNOWLEDGMENTS

The authors thank members of the Midwest Center for Structural Genomics, Argonne National Laboratory, Argonne, IL, for cloning and expression efforts, supported by National Institutes of Health Protein Structure Initiative Grant GM094585. This is manuscript 29726 from The Scripps Research Institute.

■ REFERENCES

(1) Cheng, X. C., Kihara, T., Ying, X., Uramoto, M., Osada, H., Kusakabe, H., Wang, B., Kobayashi, Y., Ko, K., Yamaguchi, I., Shen, Y., and Isono, K. (1989) A new antibiotic, tautomycetin. *J. Antibiot. 42*, 141−144.

(2) Cheng, X. C., Ubukata, M., and Isono, K. (1990) The structure of tautomycetin, a dialkylmaleic anhydride antibiotic. *J. Antibiot. 43*, 890−896.

(3) Mitsuhashi, S., Matsuura, N., Ubukata, M., Oikawa, H., Shima, H., and Kikuchi, K. (2001) Tautomycetin is a novel and specific inhibitor of serine/threonine protein phosphatase type 1, PP1. *Biochem. Biophys. Res. Commun. 287*, 328−331.

(4) Oikawa, H. (2002) Synthesis of specific protein phosphatase inhibitors, tautomycin and tautomycetin toward structure-activity relationship study. *Curr. Med. Chem. 9*, 2033−2053.

(5) Chen, X., Zheng, Y., and Shen, Y. (2007) Natural products with maleic anhydride structure: nonadrides, tautomycin, chaetomellic anhydride, and other compounds. *Chem. Rev. 107*, 1777−1830.

(6) Niu, M., Sun, Y., Liu, B., Tang, L., and Qiu, R. (2012) Differential effects of tautomycetin and its derivatives on protein phosphatase inhibition, immunosuppressive function and antitumor activity. *Korean J. Physiol. Pharmacol. 16*, 145−151.

(7) Choy, M. S., Swingle, M., D'Arcy, B., Abney, K., Rusin, S. F., Kettenbach, A. N., Page, R., Honkanen, R. E., and Peti, W. (2017) PP1: Tautomycetin complex reveals a path toward the development of PP1-specific inhibitors. *J. Am. Chem. Soc. 139*, 17703−17706.

(8) Liu, S., Yu, Z., Yu, X., Huang, S. X., Luo, Y., Wu, L., Shen, W., Yang, Z., Wang, L., Gunawan, A. M., Chan, R. J., Shen, B., and Zhang, Z. Y. (2011) SHP2 is a target of the immunosuppressant tautomycetin. *Chem. Biol. 18*, 101−110.

(9) Li, W., Luo, Y., Ju, J., Rajski, S. R., Osada, H., and Shen, B. (2009) Characterization of the tautomycetin biosynthetic gene cluster from *Streptomyces griseochromogenes* provides new insight into dialkylmaleic anhydride biosynthesis. *J. Nat. Prod. 72*, 450−459.

(10) Choi, S. S., Hur, Y. A., Sherman, D. H., and Kim, E. S. (2007) Isolation of the biosynthetic gene cluster for tautomycetin, a linear polyketide T cell-specific immunomodulator from *Streptomyces* sp. CK4412. *Microbiology 153*, 1095−1102.

(11) Luo, Y., Li, W., Ju, J., Yuan, Q., Peters, N. R., Hoffmann, F. M., Huang, S. X., Bugni, T. S., Rajski, S., Osada, H., and Shen, B. (2010) Functional characterization of TtnD and TtnF, unveiling new insights into tautomycetin biosynthesis. *J. Am. Chem. Soc. 132*, 6663−6671.

(12) Yang, D., Li, W., Huang, S. X., and Shen, B. (2012) Functional characterization of *ttnI* completing the tailoring steps for tautomycetin biosynthesis in *Streptomyces griseochromogenes*. *Org. Lett. 14*, 1302−1305.

(13) Li, T., Huo, L., Pulley, C., and Liu, A. (2012) Decarboxylation mechanisms in biological system. *Bioorg. Chem. 43*, 2−14.

(14) Leys, D., and Scrutton, N. S. (2016) Sweating the assets of flavin cofactors: new insight of chemical versatility from knowledge of structure and mechanism. *Curr. Opin. Struct. Biol. 41*, 19−26.

DOI: 10.1021/acschembio.8b00673
ACS Chem. Biol. 2018, 13, 2728−2738

(15) Marshall, S. A., Payne, K. A. P., and Leys, D. (2017) The UbiX-UbiD system: The biosynthesis and use of prenylated flavin (prFMN). *Arch. Biochem. Biophys. 632*, 209−221.
(16) Piano, V., Palfey, B. A., and Mattevi, A. (2017) Flavins as covalent catalysts: new mechanisms emerge. *Trends Biochem. Sci. 42*, 457−469.
(17) Cox, G. B., Young, I. G., McCann, L. M., and Gibson, F. (1969) Biosynthesis of ubiquinone in *Escherichia coli* K-12: location of genes affecting the metabolism of 3-octaprenyl-4-hydroxybenzoic acid and 2-octaprenylphenol. *J. Bacteriol. 99*, 450−458.
(18) Lin, F., Ferguson, K. L., Boyer, D. R., Lin, X. N., and Marsh, E. N. G. (2015) Isofunctional enzymes PAD1 and UbiX catalyze formation of a novel cofactor required by ferulic acid decarboxylase and 4-hydroxy-3-polyprenylbenzoic acid decarboxylase. *ACS Chem. Biol. 10*, 1137−1144.
(19) Payne, K. A., White, M. D., Fisher, K., Khara, B., Bailey, S. S., Parker, D., Rattray, N. J., Trivedi, D. K., Goodacre, R., Beveridge, R., Barran, P., Rigby, S. E., Scrutton, N. S., Hay, S., and Leys, D. (2015) New cofactor supports α,β-unsaturated acid decarboxylation *via* 1,3-dipolar cycloaddition. *Nature 522*, 497−501.
(20) White, M. D., Payne, K. A., Fisher, K., Marshall, S. A., Parker, D., Rattray, N. J., Trivedi, D. K., Goodacre, R., Rigby, S. E., Scrutton, N. S., Hay, S., and Leys, D. (2015) UbiX is a flavin prenyltransferase required for bacterial ubiquinone biosynthesis. *Nature 522*, 502−506.
(21) Wang, P. H., Khusnutdinova, A. N., Luo, F., Xiao, J., Nemr, K., Flick, R., Brown, G., Mahadevan, R., Edwards, E. A., and Yakunin, A. F. (2018) Biosynthesis and activity of prenylated FMN cofactors. *Cell Chem. Biol. 25*, 560−570.
(22) Marshall, S. A., Fisher, K., Ní Cheallaigh, A., White, M. D., Payne, K. A., Parker, D. A., Rigby, S. E., and Leys, D. (2017) Oxidative maturation and structural characterization of prenylated FMN binding by UbiD, a decarboxylase involved in bacterial ubiquinone biosynthesis. *J. Biol. Chem. 292*, 4623−4637.
(23) Ferguson, K. L., Arunrattanamook, N., and Marsh, E. N. G. (2016) Mechanism of the novel prenylated flavin-containing enzyme ferulic acid decarboxylase probed by isotope effects and linear free-energy relationships. *Biochemistry 55*, 2857−2863.
(24) Lan, C. L., and Chen, S. L. (2016) The decarboxylation of α,β-unsaturated acid catalyzed by prenylated FMN-dependent ferulic acid decarboxylase and the enzyme inhibition. *J. Org. Chem. 81*, 9289−9295.
(25) Ferguson, K. L., Eschweiler, J. D., Ruotolo, B. T., and Marsh, E. N. G. (2017) Evidence for a 1,3-dipolar cyclo-addition mechanism in the decarboxylation of phenylacrylic acids catalyzed by ferulic acid decarboxylase. *J. Am. Chem. Soc. 139*, 10972−10975.
(26) Arunrattanamook, N., and Marsh, E. N. G. (2018) Kinetic characterization of prenyl-flavin synthase from *Saccharomyces cerevisiae*. *Biochemistry 57*, 696−700.
(27) Tian, G., and Liu, Y. (2017) Mechanistic insights into the catalytic reaction of ferulic acid decarboxylase from *Aspergillus niger*: a QM/MM study. *Phys. Chem. Chem. Phys. 19*, 7733−7742.
(28) Bailey, S. S., Payne, K. A. P., Fisher, K., Marshall, S. A., Cliff, M. J., Spiess, R., Parker, D. A., Rigby, S. E. J., and Leys, D. (2018) The role of conserved residues in Fdc decarboxylase in prenylated flavin mononucleotide oxidative maturation, cofactor isomerization, and catalysis. *J. Biol. Chem. 293*, 2272−2287.
(29) Jacewicz, A., Izumi, A., Brunner, K., Schnell, R., and Schneider, G. (2013) Structural insights into the UbiD protein family from the crystal structure of PA0254 from *Pseudomonas aeruginosa*. *PLoS One 8*, e63161.
(30) Payer, S. E., Marshall, S. A., Bärland, N., Sheng, X., Reiter, T., Dordic, A., Steinkellner, G., Wuensch, C., Kaltwasser, S., Fisher, K., Rigby, S. E. J., Macheroux, P., Vonck, J., Gruber, K., Faber, K., Himo, F., Leys, D., Pavkov-Keller, T., and Glueck, S. M. (2017) Regioselective *para*-carboxylation of catechols with a prenylated flavin dependent decarboxylase. *Angew. Chem., Int. Ed. 56*, 13893−13897.
(31) Krissinel, E., and Henrick, K. (2007) Inference of macromolecular assemblies from crystalline state. *J. Mol. Biol. 372*, 774−797.
(32) Yang, J., Yan, R., Roy, A., Xu, D., Poisson, J., and Zhang, Y. (2015) The I-TASSER Suite: protein structure and function prediction. *Nat. Methods 12*, 7−8.
(33) Roy, A., Kucukural, A., and Zhang, Y. (2010) I-TASSER: a unified platform for automated protein structure and function prediction. *Nat. Protoc. 5*, 725−738.
(34) Zhang, Y. (2008) I-TASSER server for protein 3D structure prediction. *BMC Bioinf. 9*, 40.
(35) Morris, G. M., Huey, R., Lindstrom, W., Sanner, M. F., Belew, R. K., Goodsell, D. S., and Olson, A. J. (2009) AutoDock4 and AutoDockTools4: Automated docking with selective receptor flexibility. *J. Comput. Chem. 30*, 2785−2791.
(36) Lupa, B., Lyon, D., Gibbs, M. D., Reeves, R. A., and Wiegel, J. (2005) Distribution of genes encoding the microbial non-oxidative reversible hydroxyarylic acid decarboxylases/phenol carboxylases. *Genomics 86*, 342−351.
(37) Stratford, M., Plumridge, A., Pleasants, M. W., Novodvorska, M., Baker-Glenn, C. A., Pattenden, G., and Archer, D. B. (2012) Mapping the structural requirements of inducers and substrates for decarboxylation of weak acid preservatives by the food spoilage mould *Aspergillus niger*. *Int. J. Food Microbiol. 157*, 375−383.
(38) Gerlt, J. A. (2017) Genomic Enzymology: Web Tools for Leveraging Protein Family Sequence-Function Space and Genome Context to Discover Novel Functions. *Biochemistry 56*, 4293−4308.
(39) Dennig, A., Kuhn, M., Tassoti, S., Thiessenhusen, A., Gilch, S., Bülter, T., Haas, T., Hall, M., and Faber, K. (2015) Oxidative Decarboxylation of Short-Chain Fatty Acids to 1-Alkenes. *Angew. Chem., Int. Ed. 54*, 8819−8822.
(40) Kumar, S., Stecher, G., and Tamura, K. (2016) MEGA7: Molecular Evolutionary Genetics Analysis Version 7.0 for Bigger Datasets. *Mol. Biol. Evol. 33*, 1870−1874.
(41) Kabsch, W. (2010) XDS. *Acta Crystallogr., Sect. D: Biol. Crystallogr. 66*, 125−132.
(42) Bunkoczi, G., Echols, N., McCoy, A. J., Oeffner, R. D., Adams, P. D., and Read, R. J. (2013) Phaser.MRage: automated molecular replacement. *Acta Crystallogr., Sect. D: Biol. Crystallogr. 69*, 2276−2286.
(43) Emsley, P., and Cowtan, K. (2004) Coot: model-building tools for molecular graphics. *Acta Crystallogr., Sect. D: Biol. Crystallogr. 60*, 2126−2132.
(44) Afonine, P. V., Grosse-Kunstleve, R. W., Echols, N., Headd, J. J., Moriarty, N. W., Mustyakimov, M., Terwilliger, T. C., Urzhumtsev, A., Zwart, P. H., and Adams, P. D. (2012) Towards automated crystallographic structure refinement with phenix.refine. *Acta Crystallogr., Sect. D: Biol. Crystallogr. 68*, 352−367.
(45) Bricogne, G., Blanc, E., Brandl, M., Flensburg, C., Keller, P., Paciorek, W., Roversi, P., Sharff, A., Smart, O. S., Vonrhein, C., and Womack, T. O. (2017) *BUSTER*, version 2.10.3, Global Phasing Ltd., Cambridge, U.K.
(46) Yennamalli, R., Arangarasan, R., Bryden, A., Gleicher, M., and Phillips, G. N., Jr. (2014) Using a commodity high-definition television for collaborative structural biology. *J. Appl. Crystallogr. 47*, 1153−1157.
(47) Smart, O. S., Womack, T. O., Flensburg, C., Keller, P., Paciorek, W., Sharff, A., Vonrhein, C., and Bricogne, G. (2012) Exploiting structure similarity in refinement: automated NCS and target-structure restraints in BUSTER. *Acta Crystallogr., Sect. D: Biol. Crystallogr. 68*, 368−380.
(48) Laskowski, R. A., MacArthur, M. W., Moss, D. S., and Thornton, J. M. (1993) PROCHECK: a program to check the stereochemical quality of protein structures. *J. Appl. Crystallogr. 26*, 283−291.
(49) Chen, V. B., Arendall, W. B., III, Headd, J. J., Keedy, D. A., Immormino, R. M., Kapral, G. J., Murray, L. W., Richardson, J. S., and Richardson, D. C. (2010) MolProbity: all-atom structure validation for macromolecular crystallography. *Acta Crystallogr., Sect. D: Biol. Crystallogr. 66*, 12−21.

DOI: 10.1021/acschembio.8b00673
ACS Chem. Biol. 2018, 13, 2728−2738